One-Step Analysis of DNA/Chitosan Complexes by Field-Flow Fractionation Reveals Particle Size and Free Chitosan Content

Pei Lian Ma,[†] Michael D. Buschmann,[†] and Françoise M. Winnik*[,‡]

Department of Chemical and Biomedical Engineering, Ecole Polytechnique de Montréal, PO 6079 Succ. Centre-Ville, Montreal, Quebec, H3C 3A7, Canada, and Department of Chemistry and Faculty of Pharmacy, Université de Montréal, PO 6128 Succ. Centre-Ville, Montreal, Quebec, H3C 3J7, Canada

Received November 27, 2009; Revised Manuscript Received January 31, 2010

The composition of samples obtained upon complexation of DNA with chitosan was analyzed by asymmetrical flow field flow fractionation (AF4) with online UV−visible, multiangle light scattering (MALS), and dynamic light scattering (DLS) detectors. A chitosan labeled with rhodamine B to facilitate UV−vis detection of the polycation was complexed with DNA under conditions commonly used for transfection (chitosan glucosamine to DNA phosphate molar ratio of 5). AF4 analysis revealed that 73% of the chitosan-rhodamine remained free in the dispersion and that the DNA/chitosan complexes had a broad size distribution ranging from 20 to 160 nm in hydrodynamic radius. The accuracy of the data was assessed by comparison with data from batch-mode DLS and scanning electron microscopy. The AF4 combined with DLS allowed the characterization of small particles that were not detected by conventional batch-mode DLS. The AF4 analysis will prove to be an important tool in the field of gene therapy because it readily provides, in a single measurement, three important physicochemical parameters of the complexes: the amount of unbound polycation, the hydrodynamic size of the complexes, and their size distribution.

Introduction

A variety of nonviral gene delivery vectors are being investigated intensively in chemical laboratories and in clinical settings.[1] The high level of interest in these systems is motivated by the greater safety of synthetic DNA vectors compared to viral vectors and by the ease of their preparation. Indeed, condensation of DNA into positively charged nanoparticles spontaneously occurs upon mixing DNA and a polycation as a result of electrostatic attraction. The resulting dispersion may be used directly in transfection experiments or subjected to physicochemical analysis. The size distribution of DNA/polycation complexes is accessible via conventional techniques, including dynamic light scattering (DLS), microscopy, and analytical ultracentrifugation (AUC). DLS measures the time-dependent fluctuations of the light scattered by the particles to derive their hydrodynamic sizes. For samples having a broad polydispersity in size, DLS may not be able to detect small changes in the size distributions. The presence of large particles and small amounts of aggregates can mask the light scattered by the smaller particles, limiting their detection. Microscopic techniques such as AFM, SEM, and TEM have been very useful in visualizing the particles and characterizing their size and morphology, but they often require sample drying and the use of contrast staining agents that can influence the properties of the particles. The hydrodynamic size and size distribution can be obtained with AUC, but this technique requires the knowledge of the specific volume of the hydrated particles.[2] Asymmetrical flow field-flow fractionation (AF4), an analytical separation technique in which the retention of macromolecules and particles is governed by their diffusivities, is rarely used for the size determination of gene delivery systems, despite its wide applicability in colloidal science. Comparatively few studies have been published to date on the AF4 analysis of gene and drug delivery systems, including polyelectrolyte complexes,[3,4] DNA/cationic lipid complexes,[5] virus-like particles,[6] and other types of nanoparticle drug carrier systems.[7−11] This technique was used alone or combined with other detectors to obtain the particle size, the size distribution, and the molar mass distribution of monodisperse and polydisperse samples.

It is generally accepted that optimal transfection is achieved when the DNA condensation is performed in the presence of a large excess of amine groups (N/P ≥ 5, the molar ratio of chitosan protonable amine groups to DNA phosphate groups).[12−14] Under these conditions, it can be expected that a significant amount of unbound polycation coexists in the dispersion with the DNA/polycation complexes. Recent experimental data from fluorescence correlation spectroscopy (FCS)[15] and size exclusion chromatography (SEC)[12] confirmed that, in DNA/poly(ethyleneimine) (PEI) complexes prepared at N/P ratios above 6, the majority of the PEI molecules are not bound to DNA. The free PEI was nonetheless seen to be important because it was found to increase substantially the level of gene expression and was suggested to contribute to the proton sponge effect, leading to greater endosomal release of the complexes.[12] In another study, a large excess of free chitosan was detected, but not quantified, by FCS in preparations of DNA/chitosan complexes.[16] These findings highlight the importance for the quantification of the amount of uncomplexed free polycation that still remains an analytical challenge. The FCS technique can provide quantitative data on the free polycation content, but it relies on the use of mathematical models to fit the autocorrelation data of the dispersion, assuming the presence of two different species (free and bound polycation).[15] The separation method with SEC for these polydisperse samples is fraught with technical difficulties, such as loss of material, column blockages, and shearing of large particles. Moreover, it is necessary to perform a colorimetric

* To whom correspondence should be addressed. Tel.: 1-514-340-5179. E-mail: francoise.winnik@umontreal.ca.
[†] Ecole Polytechnique de Montréal.
[‡] Université de Montréal.

10.1021/bm901345q
Published on Web 02/16/2010

assay on isolated fractions to determine the concentration of free polycation in each fraction.

We report here a new approach to characterize DNA/polycation complexes using asymmetrical flow field-flow fractionation (AF4) coupled online with UV/vis spectroscopy, multiangle light scattering, and dynamic light scattering. In addition to the determination of size and size distribution, this multimodal AF4 system was optimized for the direct quantification of the free polycation content. Chitosan was selected as the polycation because it is a prominent natural polymer used in gene delivery, due to its biocompatibility and biodegradability. The relationship between transfection efficiency and physicochemical factors, including the molecular weight, the degree of deacetylation, the N/P ratio, and the solution pH, have been extensively studied.[13,17−20] These parameters were to influence the physicochemical and biological properties of DNA/chitosan complexes. The resulting surface charge, particle size, and colloidal stability of DNA/polycation complexes are interrelated properties that, in turn, have a strong impact on transfection efficiency. A complete characterization of the physicochemical properties of DNA complexes with polycations, such as chitosan, is therefore essential to define the structure−activity relationship for the optimization of gene delivery systems. The aim of this study was to demonstrate the feasibility of this combined AF4 system to separate free chitosan from DNA/chitosan complexes and to determine directly the particle size, the size distribution, and the free chitosan content in a single run. We describe briefly the principle of the AF4 method in the experimental section. The design of the separation protocol is then presented followed by the description of the outcome of the analysis in terms of size and size distribution of the complexes and of the content of unbound polycation. Results of the AF4 analysis are then directly compared with data gathered by DLS and ESEM analysis of the same samples.

Materials and Methods

Materials. The 6.4 kb plasmid EGFPLuc (Clontech Laboratories) was amplified in DH5α bacteria and purified using the Qiagen Plasmid Mega Kit. A stock solution of EGFPLuc (0.33 mg/mL) was prepared in deionized water and stored at −20 °C before use. Ultrapure chitosan (150000 g/mol, degree of deacetylation (DDA): 80%) was provided by Biosyntech Inc. It was degraded according to Lavertu et al.[13] using nitrous acid to achieve a number-average molecular weight (M_n) of 42000 g/mol and a polydispersity index of 1.35 (determined by GPC[21]). Rhodamine B-labeled chitosan (Ch-rho, M_n = 42000 g/mol, DDA = 80%, 1.2% mole of rhodamine/mol of glucosamine) was prepared following a previously reported procedure[22] (see Supporting Information for details).

Preparation of DNA/Chitosan Complexes. Unlabeled and labeled chitosan stock solutions of 5 mg/mL were prepared by dissolving the samples overnight in deionized water containing hydrochloric acid (from 1 M aq HCl solution), such as to reach an HCl/glucosamine ratio of 1. DNA and chitosan stock solutions were diluted with deionized water to concentrations of 82.5 μg/mL and 283 μg/mL, respectively. The DNA/chitosan complexes were prepared by adding 100 μL of the diluted chitosan solution to an equal volume of the diluted DNA solution to reach a glucosamine to phosphate groups (N/P) ratio of 5 in the final dispersion. The mixing was done quickly by up and down pipetting of the dispersions. Samples were allowed to incubate at room temperature 30 min before analysis.

AF4/UV/MALS/DLS System. *Instrumentation.* An asymmetrical flow field-flow fractionation (AF4) system (AF 2000 MT, Postnova Analytics) with a channel thickness of 350 μm fitted with a regenerated cellulose membrane (10 kDa cutoff; Z-MEM-AQU-631, RC amphiphilic, Postnova Analytics) suitable for analysis of amphiphilic or cationic polymers was used. The AF4 was connected online to an UV/vis detector (SPD-20A, Postnova Analytics), a multiangle light scattering detector (MALS, Dawn 8+, Wyatt Technology), and a dynamic light scattering (DLS) detector (WyattQELS, Wyatt Technology) connected to the 108° angle of the MALS Dawn 8+ detector. The MALS was equipped with a K5 cell and a GaAs laser operating at 658 nm. The samples were measured at 1 s intervals for the MALS and 3 s intervals for the DLS. The UV, MALS, and DLS signals were simultaneously recorded as fractograms, plots of detector signal intensity versus time. Data collection and analysis were done using ASTRA version 5.3.4.14 (Wyatt Technology). The online DLS detector equipped with an avalanche photodiode measures the autocorrelation function for every slice of 3 s eluting from the AF4. Each fractionated slice of 3 s contains a narrow distribution of sizes, so that the autocorrelated function for a dilute and monodisperse population can be analyzed leading to the diffusion coefficient of the corresponding slice.[23] The hydrodynamic radius (R_H) of the assumed sphere is then calculated according to the Stokes−Einstein equation. Each curve shown is representative of triplicate samples.

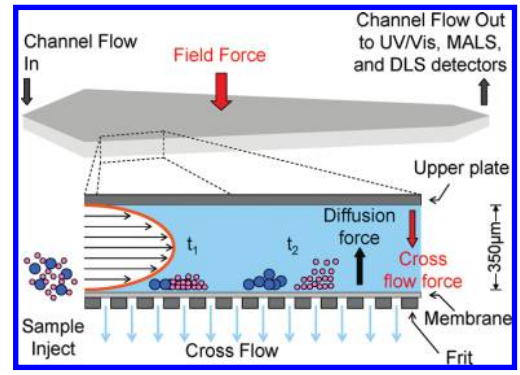

Figure 1. Schematic representation of the separation process at different elution times ($t_2 > t_1$) in an AF4 channel.

Separation Principle. The theory of asymmetrical flow field-flow fractionation (AF4) has been discussed in detail elsewhere.[24,25] The fractionation of a sample containing different species occurs in a thin and open trapezoidal channel as illustrated in Figure 1. After focusing and relaxation of the sample species, the flow along the channel drives the sample to the outlet. This channel flow is laminar with a parabolic flow profile having layers of different velocities. The highest flow rate is in the center of the channel and the lowest flow rate along the wall. An external field generated by the cross-flow and applied perpendicularly to the channel flow drives the sample toward the accumulation wall. However, diffusion opposes this field, causing migration of the sample species away from the wall. The cross-flow leaves the channel through an ultrafiltration membrane covering the accumulation wall. The molecular cutoff of the membrane is chosen such that the analyzed species cannot penetrate the membrane. Because small particles have higher diffusion coefficients, they achieve equilibrium positions which on the average lie within the channel flow layers of higher velocity, while larger particles reach equilibrium in flow layers of lower velocity. Consequently, in the normal mode of separation, small species are transported faster and are eluted prior to larger species, the latter being closer to the membrane.

Separation Conditions. A prefiltered 50 mM acetic acid/sodium acetate buffer at pH 4.0 was used as the eluent. The total ionic strength was adjusted to 20 mM by addition of NaCl. After flow equilibration, the sample (21 μL) was injected with a flow rate of 0.2 mL/min, followed by a 9 min focusing with a cross-flow rate and a detector flow rate of 1 mL/min each. Following a 1 min transition, a four-step, cross-flow rate gradient was initiated for the elution mode. The starting flow rate (1 mL/min) was decreased exponentially first with an exponent factor of 0.4 to 0.4 mL/min within 10 min, then with an exponent factor of 0.8 from 0.4 to 0.15 mL/min within 20 min, and finally it was decreased linearly from 0.15 to 0.05 mL/min within 15 min. The cross-flow rate was then kept constant at 0.05 mL/min for 15 min. The

detector flow rate was kept at 1 mL/min throughout. All the flow rates were controlled by the AF2000 Control software (Postnova Analytics). The cross-flow was generated by Kloehn syringe pumps (Postnova Analytics), while the axial and focusing flows were delivered by isocratic pumps (PN1130, Postnova Analytics).

Mass Recovery and Quantification of Free Chitosan. The mass recovery of pure Ch-rho solutions was determined and from the AF4 fractograms monitored by UV/vis detection at 556 nm. The eluted mass was calculated from the integrated peak area and the extinction coefficient of Ch-rho determined prior to conducting the AF4 experiments. The extinction coefficient of Ch-rho was 3.477 mL/(mg·cm) at 556 nm, calculated based on a calibration curve. The mass recovery was determined by comparing the calculated mass of Ch-rho with the injected mass. The mass recovery of Ch-rho was constant for at least 60 injections. For the quantification of unbound free Ch-rho in a DNA/Ch-rho dispersion, the integrated areas under the curve of the corresponding peak before and after complexation were compared. The results reported are the average (±standard deviation) of three independent measurements.

Scanning Electron Microscopy. An environmental scanning electron microscope (Quanta 200 ESEM FEG, FEI) was used to image fractions of DNA/chitosan complexes collected from AF4 separations. The fractions were collected from the outlet flow of the detectors for various elution times. A drop (10 μL) of a fraction was deposited on freshly cleaved mica, left to dry for 30 min, and then sputter-coated with gold (Agar Manual Sputter Coater, Marivac Inc.). Observations were performed at 20 kV in the high vacuum mode of the ESEM microscope. The average particle size (±standard deviation) was determined by measuring the diameter of more than 150 particles from at least 6 different fields for each fraction using the microscope XT Docu software.

Batch Mode Dynamic Light Scattering. Size measurements of the DNA/chitosan complexes before fractionation were carried out using an ALV/CGS-3 Compact Goniometer System equipped with a 22 mW HeNe laser operating at a wavelength of 632.8 nm. The complexes were diluted 4 times in the running buffer prior to analysis. The correlation functions were measured at 25 °C over an angular range between $\theta = 40$ and 150°. For each scattering angle, a second-order cumulant fit was then applied to the data to obtain the first cumulant (Γ),which is related to the diffusion coefficient (D) by $\Gamma = Dq^2$, where $q = (4\pi n/\lambda_0)\sin(\theta/2)$, with n, λ_0, and θ being the solvent refractive index, the wavelength of the incident light in vacuum, and the scattering angle, respectively. The diffusion coefficient of the particles was determined by extrapolation to zero scattering angle from a plot of Γ/q^2 versus q^2. The z-average hydrodynamic radius was calculated from the diffusion coefficient and the Stokes−Einstein equation. The data were also analyzed using the CONTIN regularized fit to determine the particle size distribution.

Results and Discussion

Optimization of the Analytical Conditions. To obtain reliable and reproducible separations, it is critical to ensure that the eluting species do not interact with the membrane or permanently adhere to it. We found that a special regenerated cellulose membrane designed for the separation of amphiphilic or cationic polymers was well-suited for the analysis of positively charged DNA/chitosan complexes in an acetic acid/acetate running buffer of pH 4 and low ionic strength. The running buffer does not alter the physical properties of the DNA/chitosan complexes initially prepared in a solution pH of 4.8. At pH 4, the residual unbound chitosan is fully ionized and can be detected and quantified, since it does not adhere onto the membrane. The experimentally determined Ch-rho mass recovery (87 ± 2%) upon injection of a Ch-rho solution confirmed that the loss of chitosan and cationic DNA/chitosan nanoparticles by adsorption was indeed negligible. The detection of unbound negatively charged DNA is not possible under these conditions, due to irreversible adsorption of DNA on the membrane observed in control studies involving injections of DNA solutions. A complete lack of UV and LS signals was observed during the AF4 separation as well as during the flushing at zero cross-flow. Since an excess of chitosan was used to prepare the complexes (N/P ratio of 5), all the DNA was bound to chitosan, as confirmed by ethidium bromide gel electrophoresis experiments.[26] The mass recovery of DNA in the complexes was estimated to be about 95% from the integrated peak area of the complexes under the curve of the UV signal at 260 nm and using the extinction coefficient of DNA. We tested other membranes, such as the commonly used and regular regenerated cellulose membrane, but the results were erratic, presumably as a consequence of massive eluate adsorption.

The four-step field gradient was optimized for the separation of free chitosan from DNA/chitosan complexes. The first exponential decrease of the cross-flow from 1.0 to 0.4 mL/min within 10 min was applied to allow the elution of free chitosan. The cross-flow was then decreased slowly in the following steps to obtain a good resolution for the fractionation of the complexes without inducing particle−particle interactions in an extent that would affect the elution times and peak shape of the fractograms. The elution of the species was complete in less than 60 min after which the cross-flow was reduced to zero and no signal was observed. The sample concentration and injected volume were chosen to obtain a high signal-to-noise ratio. The elution times and peak shape of the fractograms did not change when the sample concentration was decreased, confirming the appropriateness of the separation conditions and the absence of undesirable sample overloading effects.

Free Chitosan Content in a Dispersion of DNA/Ch-rho Nanoparticles of N/P = 5. The AF4 separation of free chitosan from DNA/Ch-rho complexes was monitored via UV detection of the eluting fractions. Since the UV absorbance of chitosan occurs at wavelengths <210 nm, a spectral region where DNA also absorbs light, it was necessary to use a chitosan labeled with a small fraction of a dye that absorbs light at wavelengths for which DNA is transparent. We selected a Ch-rho sample with a labeling level of 1.2% mole of rhodamine/mol of glucosamine and a maximum absorbance at 556 nm. Prior to the fractionation, we have verified that the size of the DNA/chitosan complexes is not affected by the labeling (see below). Elution profiles recorded at 556 and 260 nm for a solution of Ch-rho (dashed line) and for a dispersion of DNA/Ch-rho nanoparticles (full line) are presented in Figure 2. Ch-rho elutes between 1 and 9 min (dashed lines in Figure 2A (556 nm) and B (260 nm)). Profiles recorded for DNA/Ch-rho complexes (full line) present a band at longer elution times, between 8 and 32 min, attributed to the elution of the complexes, in addition to the band due to Ch-rho. Focusing on the profiles recorded at 556 nm (Figure 2A), we note that the intensity of the faster eluting band is significantly lower for the dispersion of DNA/Ch-rho complexes, compared to the Ch-rho solution. Moreover, there is a weak band eluting from about 10 to 25 min (Figure 2A), which can be attributed to the absorbance at 556 nm of Ch-rho entrapped in the complexes. Rhodamines in aqueous media are well-known to undergo spectroscopic changes due to aggregation, mainly by dimerization.[27,28] This may be induced upon the compaction of DNA by Ch-rho since rhodamine moieties are brought closer together. Rhodamine aggregation is usually accompanied by a significant hypochromic effect of the absorbance centered around 556 nm[27] and could account for the lack of signal of the nanoparticles at this wavelength.

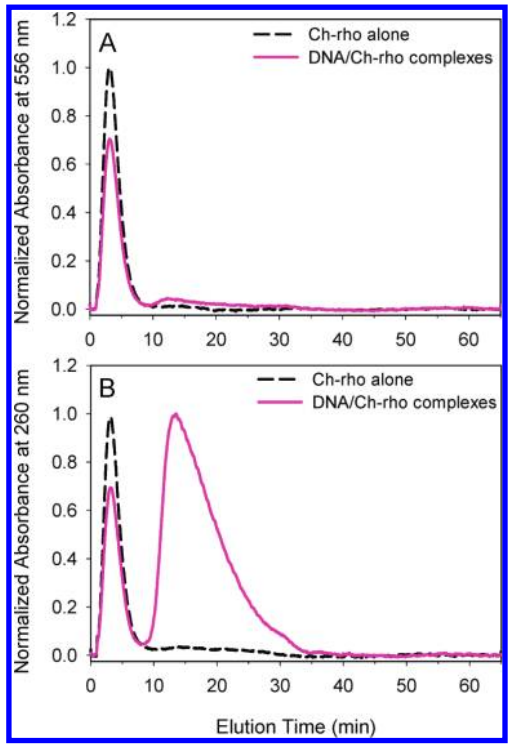

Figure 2. AF4 fractograms of chitosan-rhodamine and DNA/chitosan-rhodamine monitored by UV/vis showing (A) normalized absorbance at 556 nm and (B) normalized absorbance at 260 nm as a function of the elution time.

This observation is in agreement with the decrease of the absorption band of Ch-rho around 556 nm when comparing the absorption spectra of Ch-rho and DNA/Ch-rho prior to the separation (see the SI, Figure SI-1). Further evidence for the formation of nanoparticles was obtained by monitoring the elution with a MALS detector (see below).

Comparison of the areas of the elution bands of Ch-rho before and after complexation (Figure 2A, 556 nm) revealed that 73% (±2%) of Ch-rho is in the free form. The remainder of Ch-rho that is not free is bound to DNA. It follows that the N/P ratio in the complexes themselves is 1.4 (±0.1), although the nominal N/P ratio is 5, based on the Ch-rho and DNA amounts used to prepare the complexes. This finding is in good agreement with previous reports on DNA/PEI complexes prepared at a N/P ratio of 6 for which fluorescence correlation spectroscopy analysis indicated that 86% of the PEI is free in solution.[15] A lower value (58% of free PEI) was reported in the case of DNA/PEI complexes analyzed by a colorimetric assay following purification of the complexes by SEC.[12]

Size and Size Distribution of DNA/Ch-rho Nanoparticles. The elution of the DNA/Ch-rho complexes was monitored online using for each injection, not only a UV/vis detector, but also MALS and DLS detectors. Elution profiles of a Ch-rho solution and of a DNA/Ch-rho dispersion monitored by light scattering detectors are presented in Figure 3 which shows the normalized Rayleigh ratio at 90° (left-hand axis) and the hydrodynamic radius (R_H) of the nanoparticles (right-hand axis). The intense light scattering signal from 9 to 32 min is attributed to the complexes. The elution time of the complexes detected by MALS corresponds exactly to the elution time recorded by UV at 260 nm (Figure 2B). The chitosan molecules are too small to scatter light significantly at the concentration used. Hence they were not detected by MALS and DLS under our experimental conditions. If the characterization of chitosan is desired, the use of concentrated chitosan solutions will enable such detection, as shown in previous reports combining AF4 with MALS to determine molar masses of chitosan and its derivatives.[29,30]

Generally, the hydrodynamic radius can be calculated from the elution time based on the theory of field flow fractionation.[25] However, the retention time of the sample could be affected by interactions of charged particles with the membrane or between charged particles. Thus, we chose to calculate absolute values of the hydrodynamic size of the nanoparticles directly from data gathered via the online DLS detector. For each eluted fraction, the autocorrelated function from DLS leads to the diffusion coefficient of the particles from which the hydrodynamic radius was calculated. From the DLS fractograms (Figure 3), it can be seen that the DNA/Ch-rho nanoparticles are polydisperse in size with a hydrodynamic radius ranging from 20 to 160 nm. It should be noted that the profile of the hydrodynamic radius with the elution time is not linear because of the cross-flow exponential decays used for the AF4 separation. As mentioned above, the separation conditions were appropriately optimized to avoid effects caused by particle interactions. The different elution times demonstrate the ability of AF4 to separate different species based on their hydrodynamic size. Smaller particles having higher diffusion coefficients are less retained by the cross-flow in the channel and elute prior to the larger particles. The validity of the online DLS data was confirmed by ESEM imaging of several AF4 fractions collected after different elution times. Micrographs of three fractions are presented in Figure 3 showing nanoparticles having a spherical shape. The mean radii of the particles measured on ESEM images collected at the time intervals from 12 to 14, 16 to 18, and 28 to 30 min are, respectively, 27 ± 5, 41 ± 8, and 74 ± 12 nm. The radii of the first and second collected fractions are similar to the values obtained from the online DLS detection. However, smaller particle sizes are obtained from image analysis of the fraction collected last. Such discrepancy is attributed, in part, to the fact that DLS measures the hydrodynamic size of the charged particles assumed to be hydrated spheres, whereas dried particles are characterized by ESEM. Drying and imaging in high vacuum of the samples can also change the particle properties and cause shrinking of the particles, as reported in previous studies.[2,31] Because the sample is polydisperse in size, the nanoparticles may have different properties and be subjected differently to drying and high vacuum conditions. Further analysis of collected fractions within the same sample by other means can provide information about the difference in their physical properties other than size (zeta potential, composition, density, etc.). We did not succeed to measure the zeta potential of collected fractions because the particles recovered were too diluted.

The fact that the majority of the DNA/chitosan complexes have an elution time in the 11−20 min range and hydrodynamic radii of about 30−50 nm can also be inferred from the fractograms monitored by UV absorbance at 260 nm (Figure 2B) and online DLS (Figure 3). Focusing on the elution of the nanoparticles, data from these fractograms were converted to a size distribution shown in Figure 4, presented by plots of the cumulative and differential weight fraction as a function of the particle hydrodynamic radius. The concentration of nanoparticles was assumed to be proportional to the absorbance at 260 nm. To ascertain the validity of this assumption, we verified that the shape of the curves does not change with the sample concentration (at a constant N/P ratio of 5, injected DNA concentration from 21 to 41 μg/mL) and that the corresponding peak areas of the eluting nanoparticles follow the Beer−Lambert

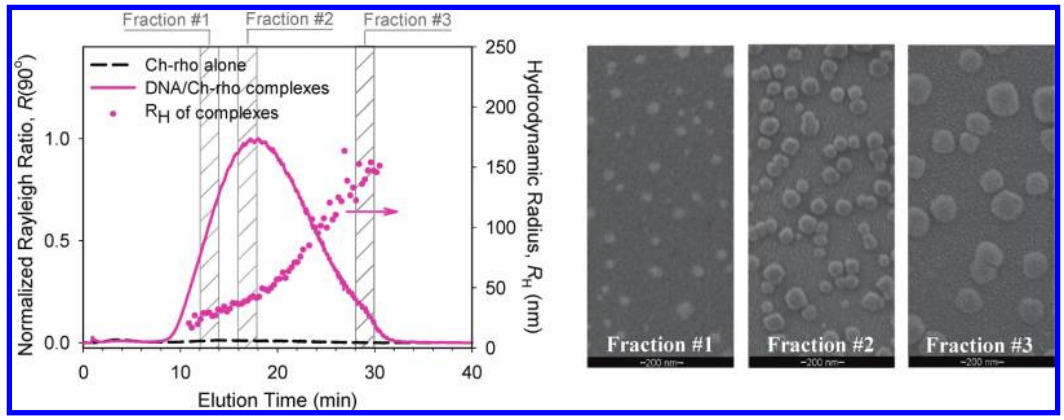

Figure 3. AF4 fractograms of chitosan-rhodamine and DNA/chitosan-rhodamine complexes with the lines and the dots representing the normalized Rayleigh ratio at 90° and the hydrodynamic radius (from online DLS) as functions of the elution time, respectively. The micrographs are ESEM images of the collected fractions of DNA/chitosan−rhodamine complexes eluted between: fraction #1, 12−14 min; fraction #2, 16−18 min; and fraction #3, 28−30 min.

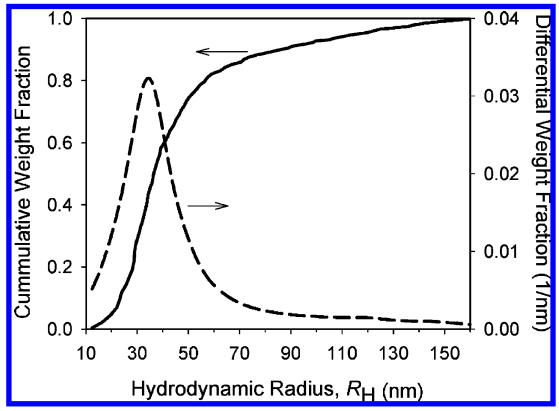

Figure 4. Cumulative and differential weight fraction from online DLS and absorbance (260 nm) measurements of AF4 fractionated DNA/Ch-rho nanoparticles.

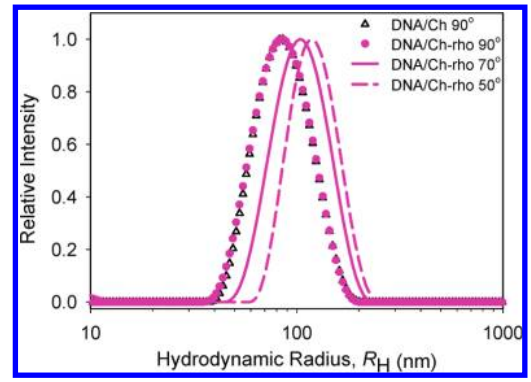

Figure 5. Intensity distribution of the hydrodynamic radius of unfractionated complexes of DNA with unlabeled chitosan (Ch) and chitosan-rhodamine (Ch-rho). The DLS measurements were carried out in batch mode at different scattering angles.

relation (see SI, Figure SI-2a and b). Because the nanoparticles are highly diluted in the flowing eluent, turbidity at this wavelength should be negligible compared to the absorption of DNA. The predominant range of particle hydrodynamic radius was 30−55 nm with about 10% of the particles having an R_H above 90 nm and about 10% with R_H less than 25 nm. The ability to provide size distribution and to fractionate particles according to size using AF4 with these combined detectors will be useful to correlate complex size with transfection efficiency.

It is common practice to assess the average size of DNA/polycation nanoparticles from DLS data (batch mode) of the dispersion obtained upon mixing polycations and DNA solutions. We carried out this measurement for a DNA/Ch-rho sample prior to AF4 analysis. Figure 5 shows the intensity distributions of hydrodynamic radii of this sample determined at three different angles. The angular dependence of the corresponding apparent diffusion coefficient is a consequence of the sample polydispersity. The *z*-averaged hydrodynamic radius was 130 nm, calculated from the Stokes−Einstein equation and the zero-angle extrapolated diffusion coefficient (see the SI, Figure SI-3). The ranges of R_H values (about 40 to 300 nm) measured at several angles by batch DLS are larger than the range of R_H values extracted from the AF4 online DLS detection and confirmed via ESEM imaging of fractions collected throughout the elution. Both the online and batch mode DLS measurements yield the overall range of hydrodynamic radii, but the contribution of the large particles to the scattered light detected by the batch mode DLS is significant, yet larger particles were found to represent only a small fraction of the sample by the combined AF4 system. Since the nanoparticles are separated by AF4 on the basis of their size *prior to DLS measurement*, the data analysis does not suffer from interference from the scattering of trace amounts of larger particles or aggregates, contrary to the situation for DLS in batch mode, for which particle size distribution is always biased toward larger particles. Also presented in Figure 5 is the size distribution of DNA/Ch nanoparticles obtained upon mixing DNA and unlabeled chitosan. It is identical to the size distribution recorded for DNA/Ch-rho nanoparticles, confirming that the labeling of chitosan did not alter the size distribution of the complexes. Moreover, we also confirmed that the AF4 separation was not affected by the labeling of chitosan by recording fractograms of DNA/Ch complexes monitored by the absorbance at 260 nm, MALS, and DLS. These fractograms were almost identical to those recorded for DNA/Ch-rho (Figure 6).

Conclusion

Investigations by AF4 with online UV/vis, MALS, and DLS detectors of DNA/chitosan complexes formed upon mixing of DNA and chitosan solutions have demonstrated that it is possible to obtain in a single measurement the size and the size distribution of the complexes together with the content of unbound polycation. This combination of techniques provides the particle hydrodynamic size and size distribution with high resolution since a fractionation step takes place prior to size measurement by DLS, eliminating the difficulty of detecting size in polydisperse samples in batch-mode DLS. The separation

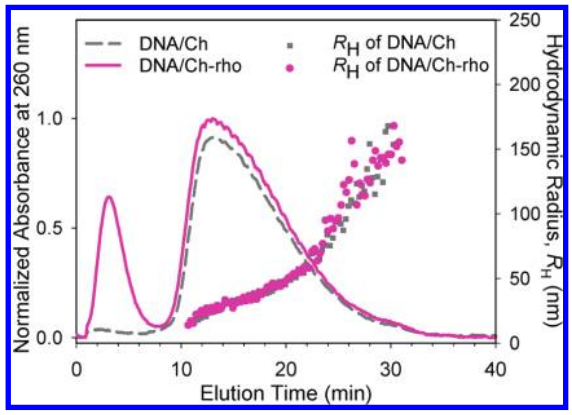

Figure 6. AF4 fractograms of DNA complexes prepared with unlabeled chitosan and chitosan-rhodamine monitored by the absorbance at 260 nm and by online DLS.

and the size measurement were confirmed by ESEM visualization of eluate fractions. Accurate quantification of unbound polycation can provide insight into the contribution of the free polycation in the process of gene delivery. An excess of positive charges is required for full DNA compaction and nuclease protection, but this constraint implies that a substantial amount of free polycation coexists with the complexes, as demonstrated in this study. The presence of free polycation is a factor to be accounted for because, on the one hand, it may improve transfection efficiency, while, on the other hand, it may also hinder cellular uptake of complexes and increase cytotoxicity and nonspecific effects, depending on the polycation type. Future studies include the characterization of DNA complexes formed with chitosans having different molecular features and with polycations other than chitosan. AF4 can also be used to separate the eluting complexes into fractions with narrow size distribution and devoid of free polycation. Analysis of the physical and biological activity of such fractions will provide new understanding of structure−activity relationships and allow optimization of the physical properties of DNA/polycation complexes for enhanced transfection efficiency.

Acknowledgment. We would like to thank Monica Nelea for ESEM imaging of the collected fractions of complexes. This work was supported by the Canadian Institutes of Health Research (CIHR) and by the Natural Sciences and Engineering Research Council of Canada (NSERC). P.L.M. received a doctoral fellowship from the Fonds québécois de la recherche sur la nature et les technologies.

Supporting Information Available. Description of the labeling of chitosan with rhodamine B isothiocyanate. Absorption spectra of DNA, Ch-rho, Ch, DNA/Ch-rho, and DNA/Ch complexes. AF4 fractograms of DNA/Ch-rho complexes at a constant N/P ratio of 5 and different sample concentrations monitored b at 260 nm. Plot of the integrated peak areas of the nanoparticles versus the DNA concentration in the samples. Extrapolation of the batch DLS data to zero scattering angle from a plot of Γ/q^2 against q^2 to determine the diffusion coefficient. This material is available free of charge via the Internet at http://pubs.acs.org.

References and Notes

(1) Mintzer, M. A.; Simanek, E. E. *Chem. Rev.* **2008**, *109*, 259–302.
(2) Bootz, A.; Vogel, V.; Schubert, D.; Kreuter, J. *Eur. J. Pharm. Biopharm.* **2004**, *57*, 369–375.
(3) Yohannes, G.; Holappa, S.; Wiedmer, S. K.; Andersson, T.; Tenhu, H.; Riekkola, M.-L. *Anal. Chim. Acta* **2005**, *542*, 222–229.
(4) Le Cerf, D.; Simon, S.; Argillier, J.-F.; Picton, L. *Anal. Chim. Acta* **2007**, *604*, 2–8.
(5) Lee, H.; Williams, S. K. R.; Allison, S. D.; Anchordoquy, T. *J. Anal. Chem.* **2001**, *73*, 837–843.
(6) Citkowicz, A.; Petry, H.; Harkins, R. N.; Ast, O.; Cashion, L.; Goldmann, C.; Bringmann, P.; Plummer, K.; Larsen, B. R. *Anal. Biochem.* **2008**, *376*, 163–172.
(7) Fraunhofer, W.; Winter, G.; Coester, C. *Anal. Chem.* **2004**, *76*, 1909–1920.
(8) Zillies, J. C.; Zwiorek, K.; Winter, G.; Coester, C. *Anal. Chem.* **2007**, *79*, 4574–4580.
(9) Jahn, A.; Vreeland, W. N.; DeVoe, D. L.; Locascio, L. E.; Gaitan, M. *Langmuir* **2007**, *23*, 6289–6293.
(10) Kang, D. Y.; Kim, M. J.; Kim, S. T.; Oh, K. S.; Yuk, S. H.; Lee, S. *Anal. Bioanal. Chem.* **2008**, *390*, 2183–2188.
(11) Augsten, C.; Kiselev, M. A.; Gehrke, R.; Hause, G.; Mäder, K. *J. Pharm. Biomed. Anal.* **2008**, *47*, 95–102.
(12) Boeckle, S.; von Gersdorff, K.; van der Piepen, S.; Culmsee, C.; Wagner, E.; Ogris, M. *J. Gene Med.* **2004**, *6*, 1102–1111.
(13) Lavertu, M.; Methot, S.; Tran-Khanh, N.; Buschmann, M. D. *Biomaterials* **2006**, *27*, 4815–4824.
(14) Strand, S. P.; Issa, M. M.; Christensen, B. E.; Varum, K. M.; Artursson, P. *Biomacromolecules* **2008**, *9*, 3268–3276.
(15) Clamme, J. P.; Azoulay, J.; Mely, Y. *Biophys. J.* **2003**, *84*, 1960–1968.
(16) Reitan, N. K.; Maurstad, G.; de Lange Davies, C.; Strand, S. P. *Biomacromolecules* **2009**, *10*, 1508–1515.
(17) MacLaughlin, F. C.; Mumper, R. J.; Wang, J.; Tagliaferri, J. M.; Gill, I.; Hinchcliffe, M.; Rolland, A. P. *J. Controlled Release* **1998**, *56*, 259–272.
(18) Koping-Hoggard, M.; Tubulekas, I.; Guan, H.; Edwards, K.; Nilsson, M.; Varum, K. M.; Artursson, P. *Gene Ther.* **2001**, *8*, 1108–1121.
(19) Ishii, T.; Okahata, Y.; Sato, T. *Biochim. Biophys. Acta Biomembr.* **2001**, *1514*, 51–64.
(20) Ma, P. L.; Lavertu, M.; Winnik, F. M.; Buschmann, M. D. *Biomacromolecules* **2009**, *10*, 1490–1499.
(21) Nguyen, S.; Winnik, F. M.; Buschmann, M. D. *Carbohydr. Polym.* **2009**, *75*, 528–533.
(22) Ma, O.; Lavertu, M.; Sun, J.; Nguyen, S.; Buschmann, M. D.; Winnik, F. M.; Hoemann, C. D. *Carbohydr. Polym.* **2008**, *72*, 616–624.
(23) Chu, B. *Laser Light Scattering: Basic Principles and Practice*, 2nd ed.; Academic Press: Boston, 1991; p 343.
(24) Wahlund, K. G.; Giddings, J. C. *Anal. Chem.* **1987**, *59*, 1332–1339.
(25) Schimpf, M. E., Caldwell, K., Giddings, J. C., Eds. *Field-Flow Fractionation Handbook*; John Wiley & Sons: New York, 2000; p 616.
(26) Strand, S. P.; Danielsen, S.; Christensen, B. E.; Varum, K. M. *Biomacromolecules* **2005**, *6*, 3357–3366.
(27) Selwyn, J. E.; Steinfeld, J. I. *J. Phys. Chem.* **1972**, *76*, 762–774.
(28) Ilich, P.; Mishra, P. K.; Macura, S.; Burghardt, T. P. *Spectrochim. Acta, Part A* **1996**, *52*, 1323–1330.
(29) Mao, S.; Augsten, C.; Maeder, K.; Kissel, T. *J. Pharm. Biomed. Anal.* **2007**, *45*, 736–741.
(30) Augsten, C.; Maeder, K. *Int. J. Pharm.* **2008**, *351*, 23–30.
(31) Lee, S.; Rao, S. P.; Moon, M. H.; Giddings, J. C. *Anal. Chem.* **1996**, *68*, 1545–1549.

BM901345Q